Disrupted Flow Memory and Synchrony in the Mekong River under Dam Regulation and Climate Change: Implications for Tonle Sap Reverse Flow

Khosro Morovati[1], Hongling Zhao[1], Fuqiang Tian[1]

[1]Department of Hydraulic Engineering & State Key Laboratory of Hydro-science and Engineering, Tsinghua University, Beijing, 100084, China

Correspondence to: Fuqiang Tian (tianfq@mail.tsinghua.edu.cn)

Abstract. Dam construction and climate change have profoundly altered the hydrological dynamics of the Mekong River-Tonle Sap Lake floodplain system, one of the world's most ecologically productive river-lake complexes. This study provides an integrated, multi-scale assessment of flow regime alteration across the Mekong mainstream and its coupling with the Tonle Sap Lake for three periods: pre-dam (1976-1991), transition (1992-2009), and post-dam (2010-2024). Using daily and sub-daily data from eight stations, we quantify shifts in long-term flow memory, short-term variability, and flow amplitude. These analyses are complemented by a hydrodynamic response-time model to evaluate how upstream regime changes propagate to the Tonle Sap-Mekong flow exchange.

We find that dam regulation and climate change have reduced spatial coherence and weakened temporal persistence of the Mekong's flow regime, indicating increasing hydrological fragmentation along the river network. Upstream stations, particularly Chiang Saen, exhibit a 33.3% increase in minimum flows and a 40% decrease in maximum flows during the post-dam period compared to the pre-dam period, alongside higher flow memory (+0.10), reflecting flow smoothing by reservoir operations. Seasonal amplitude variability remains comparatively high in the lower reach due to monsoonal tributary inflows, whereas day-to-day flashiness shows the strongest regulation signal in the upper mainstream. At the most downstream station–Kratie, a key control point for Tonle Sap inflow–maximum flows decreased by 9.4%, while minimum flows increased by 117% in the post-dam period relative to the pre-dam baseline, also delaying the seasonal timing of peak discharge by two weeks.

Critically, the combined effects of the altered flow regime and sand mining-driven riverbed lowering have altered the conditions under which Tonle Sap flow reversal initiates. Using the lag-adjusted Kratie discharge at onset as an operational proxy for the Mekong-Tonle Sap confluence stage/head condition, we find that the median onset discharge increased from ~3,000 $m^3 s^{-1}$ (pre-dam) to ~7,000 $m^3 s^{-1}$ (post-dam), an increase of >130%. This upward shift is most consistent with incision-induced changes in local stage-discharge relationships, while dam regulation and climate change primarily modulate how frequently and how persistently the reversal-favourable hydraulic gradient is exceeded, collectively shortening the reverse flow period by 24 days compared to the pre-dam period. Our findings demonstrate that preserving the Mekong's natural flood pulse and its interaction with Tonle Sap Lake will require basin-wide hydrological monitoring and

transboundary governance frameworks that account not only for volume but also for flow timing, variability, and ecological function.

1 Introduction

In riverine ecosystems, the flow regime–comprising the magnitude, timing, frequency, duration, and rate of change of discharge–is a foundational driver of ecological structure and biogeochemical functioning (Poff et al., 1997; Binh et al., 2020). Alterations to this regime, driven by climate change and intensified human interventions such as dam construction, have emerged as critical concerns within the hydrological and ecological sciences (Lao et al., 2022; Morovati et al., 2024a). Since the 1990s, global river management has shifted beyond managing total runoff volumes toward safeguarding the integrity of natural flow dynamics (Li et al., 2017). Maintaining or restoring functional flow regimes ecologically has thus become a shared priority for engineers, policymakers, and ecologists seeking to balance infrastructure development with ecosystem resilience (Yin et al., 2011; Arthington et al., 2018).

The Mekong River, one of the world's most biodiverse and socioeconomically critical transboundary rivers (Try et al., 2022), has undergone profound hydrological transformations due to the rapid expansion of hydropower infrastructure (Soukhaphon et al., 2021; Yun et al., 2024). Particularly since 2010, large-scale dam construction in the upper Mekong (Lancang) and lower Mekong tributaries has disrupted the river's natural monsoonal flood regime, fundamentally altering the hydrological connectivity that supports downstream floodplain and delta systems (Hecht et al., 2019; Morovati et al., 2026). From 2010 to 2015 alone, dam operations accounted for approximately 62% of total streamflow change in the basin (Li et al., 2017). These impacts have been especially pronounced during the dry season (November-April): Räsänen et al. (2017) reported dry season discharge increases of 121-187% at Chiang Saen, the most upstream station in our study reach, in March, and an increase of 32-46% at Kratie, the most downstream station (Fig. 1). Lu and Chua (2021) found a 98% increase in monthly discharge at Chiang Saen during the dry months. Concurrently, wet-season flows (May-October) have declined substantially (Lu et al., 2014), undermining the amplitude and timing of flood pulses that sustain floodplain ecosystems. Nguyen et al. (2025) documented a 73.7% increase in dry-season flows at Chiang Saen between 2000 and 2019, underscoring the dominant role of dam-induced regulation.

Most existing Mekong assessments emphasize changes in seasonal means, extremes, and selected indicators of alteration. However, such descriptors do not fully capture two properties that are central to how basin-wide signals propagate through a river network and translate into downstream responses: flow memory and flow synchrony. Here, flow memory refers to the persistence (long-range dependence) of discharge variability, that is, the extent to which present conditions retain information from antecedent fluctuations; we quantify this using the Hurst exponent (see Methods). Flow synchrony refers to the coherence of hydrograph timing and shape among stations along the mainstream, evaluated here using inter-station similarity of standardized daily discharge time series (see Methods). These properties are not simply statistical: memory affects how rapidly wet-season anomalies build and decay (and thus how predictable seasonal cues remain), while synchrony

reflects how coherently the flood pulse is transmitted downstream. A decline in either property indicates hydrological fragmentation, meaning that upstream forcing becomes less persistently expressed through time and less consistently aligned across space, even when changes in mean seasonal discharge appear modest.

In parallel, the effects of such disruptions on threshold-sensitive processes such as the annual reverse flow from the Mekong into Tonle Sap Lake, a globally unique hydrological phenomenon essential to Cambodian fisheries, agriculture, and biodiversity (Yoshida et al., 2020; Morovati et al., 2021) remain underexplored. Tonle Sap Lake functions as a seasonal water storage system, with reverse flows during the monsoon expanding the lake by up to sixfold (Try et al., 2020; Do et al., 2025), delivering nutrient-rich sediment and sustaining livelihoods across Cambodia (Arias et al., 2014; Morovati et al., 2023). Earlier work has shown that Mekong flow alteration can reduce flood-peak amplitude and shorten flood duration, with important ecological consequences for the Tonle Sap flood pulse (Kummu and Sarkkula, 2008). Climate variability further exerts strong control on Tonle Sap storage, with lake-volume anomalies closely tracking rainy-season rainfall anomalies across the Mekong Basin (Frappart et al., 2018), and satellite-based analyses indicate that interannual inundation fluctuations are dominated by precipitation variability, while the contribution attributed to dams constructed in China is comparatively small (Wang et al., 2020). More recently, geomorphic change near the confluence has been identified as a major control: sand-mining-driven riverbed lowering of the Mekong mainstream reduced reverse flow by ~40-50% between 1998 and 2018 (Quan et al., 2025). Building on these advances, a key remaining empirical gap is to quantify how the discharge conditions associated with the onset and cessation of reverse flow have shifted over multiple decades, and to link those threshold shifts to basin-wide reorganization of flow persistence (memory) and spatial coherence (synchrony) observed along the mainstream.

A wide range of approaches, including statistical indicators, hydrodynamic simulations, and hydrological models, have been employed to assess flow regime alterations in the Mekong basin (Delgado et al., 2010; Lauri et al., 2012; Piman et al., 2013; Cochrane et al., 2014; Li et al., 2017; Yun et al., 2020; Lu and Chua, 2021; Wang et al., 2021; Chen et al., 2021). Among these, the Indicators of Hydrologic Alteration (IHA) framework remains one of the most widely used tools for evaluating site-specific changes in hydrologic parameters (Li et al., 2017; Binh et al., 2020). However, IHA's predominantly univariate and station-based nature limits its ability to capture system-wide dynamics, such as spatial coherence, inter-station synchrony, or long-term predictability. This limitation is particularly critical in the Mekong basin, where pronounced spatial and temporal variability in precipitation (Pokhrel et al., 2018; Zhang et al., 2023), combined with the presence of over 300 operational dams–and, according to some sources, more than 500 (Ang et al., 2024)–has resulted in extensive flow regulation. To address these gaps, alternative metrics have been proposed. The Richards-Baker (R-B) Flashiness Index, for example, captures short-term variability by quantifying how rapidly flow rises and falls (Gannon et al., 2022), while the Hurst exponent provides a measure of long-range dependence or memory in discharge time series.

This study addresses these gaps through a multi-decadal, multi-indicator assessment of flow regime shifts at eight mainstream stations along the Mekong River from 1976 to 2024. We quantify changes in daily discharge variability, flashiness, and memory across three hydrological periods: pre-dam (1976-1991), transition (1992-2009), and post-dam

(2010-2024), introducing the concepts of disrupted flow memory and fragmented synchrony to describe the breakdown in spatiotemporal coherence. In addition to these indicators, we examine annual discharge extremes, including maximum and minimum daily flows and their associated timing. In addition, using 15-min water-level observations (2018-2025), we quantify sub-daily variability using amplitude, flashiness (RBI), and peak count metrics. Finally, we link these altered flow characteristics to the onset, termination, and duration thresholds of Tonle Sap's reverse flow using Delft3D-Flow hydrodynamic simulations with a response-time model from Kratie to the Mekong-Tonle Sap confluence (Fig. 1b), which enables a physically consistent lag adjustment between Kratie discharge and conditions at the confluence. This approach enables the empirical derivation of reverse flow thresholds and reveals significant temporal shifts in both their magnitude and timing. Our findings highlight the intensifying influence of recent dam developments, together with the impacts of climate change, and provide updated, system-wide insights for hydrological management within the frameworks of the Mekong River Commission (MRC) and the Lancang-Mekong Cooperation (LMC), where effective science-policy communication is essential (Orieschnig et al., 2026; Morovati et al., 2026).

2 Materials and methods

2.1 Study area

The Mekong River, one of the world's most prominent transboundary river systems, extends over 4,800 km from the glaciated Tibetan Plateau through six countries–China, Myanmar, Laos, Thailand, Cambodia, and Vietnam–before discharging into the sea (Duc et al., 2020). Over the past three decades, hydrological dynamics in the basin have been reshaped by the combined pressures of climate change and rapid hydropower expansion. Shifts in precipitation regimes and temperature variability have interacted with extensive dam construction on both the mainstream and tributaries (Ang et al., 2024), amplifying alterations to the river's seasonal flow regime. Twelve large dams are now located on the upper Mekong (Lancang) in China (Fig. 1a), with a collective storage capacity exceeding 43,000 million m^3 (Mm^3). Among them, the Xiaowan (14,645 Mm^3, completed in 2010) and Nuozhadu (21,749 Mm^3, completed in 2014) reservoirs dominate in both scale and operational influence (Zhang et al., 2023).

In the lower Mekong, mainstream dam development began more recently, marked by the commissioning of the Xayaburi Dam in 2019 and the Don Sahong Dam in 2020, together contributing around 1,300 Mm^3 of storage (Fig. 1a). Although many of the tributary dams are small (<5 km^3), their cumulative storage, asynchronous operational strategies, and often uncoordinated management (Lyu et al., 2024; Morovati et al., 2024b)–even within a single jurisdiction–have led to profound disruptions in the basin's natural flow regime (Morovati et al., 2026). These hydrological shifts are further intensified by the region's pronounced spatial and temporal variability in precipitation, including extreme monsoonal rainfall patterns typical of the lower Mekong's tropical climate (Pokhrel et al., 2018; Zhang et al., 2023).

Downstream, the Mekong River interacts seasonally with the Tonle Sap Lake via the Tonle Sap River. During the wet season, elevated mainstream water levels reverse the hydraulic gradient at the confluence and drive reverse flow into the

lake, expanding its surface area from ~2,500 km² in the dry season to > 13,000 km² at peak inundation (Kummu et al., 2014; Morovati et al., 2023). Lake water level typically rises from ~1.2 to 10.4 m (Dang et al., 2022), corresponding to a storage increase of ~1.6-59.7 km³ (Kummu et al., 2014; Morovati et al., 2023). Water-balance analyses indicate that the Mekong mainstream (via reverse flow) supplies the dominant fraction of annual inflow (~42-53.5%), while Tonle Sap tributaries contribute a smaller but substantial share (~34-41%), and direct precipitation contributes ~12.5% (Kummu et al., 2014; Morovati et al., 2023). This seasonal exchange delivers sediment- and nutrient-rich water that underpins floodplain productivity, supporting one of the world's most productive freshwater fisheries and sustaining Cambodia's rice-based agrarian economy.

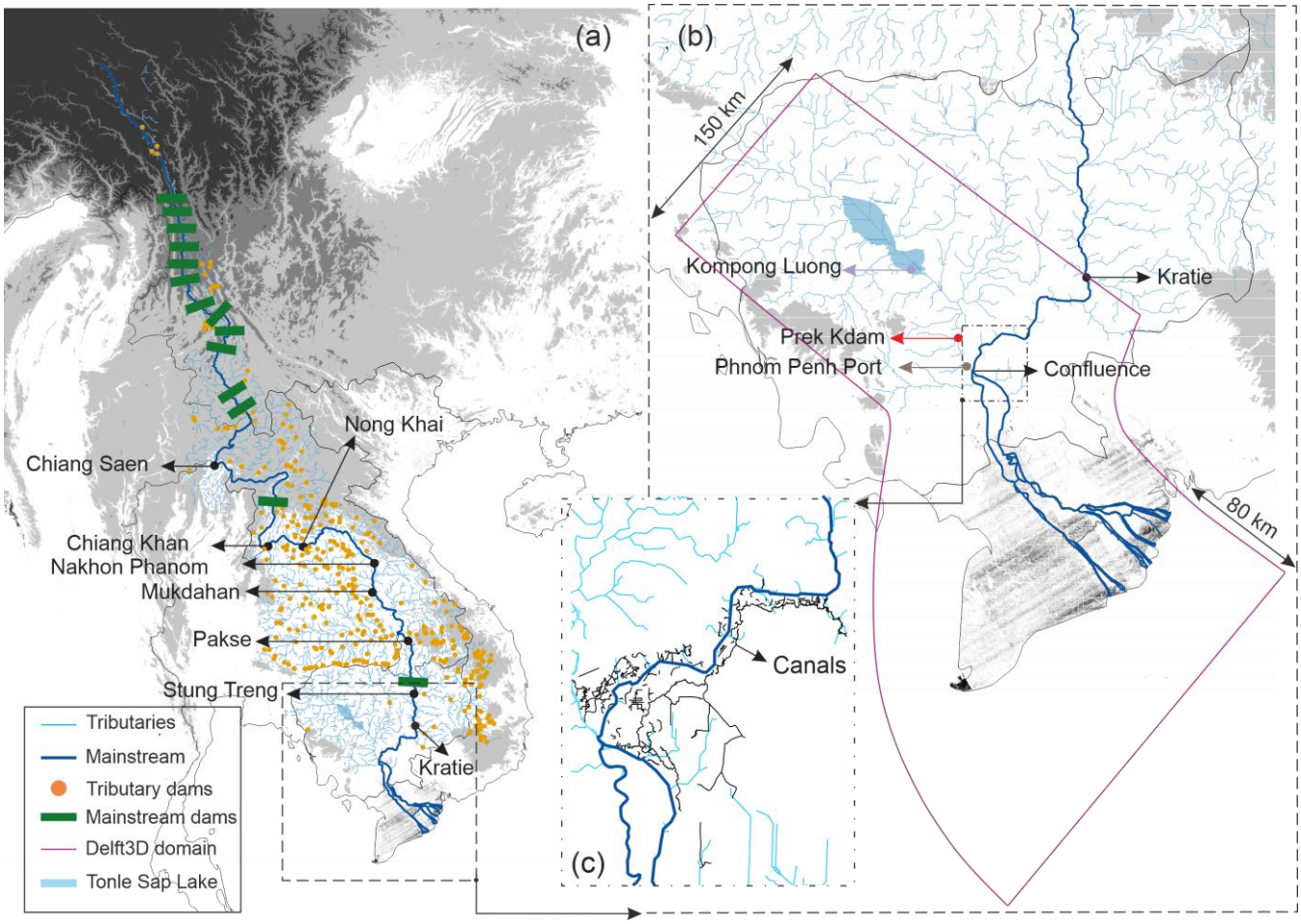


Figure 1. Map of the Mekong River basin and model configuration. (a) Locations of the Mekong mainstream and tributary network, hydrological stations, and mainstream and tributary dams. (b) Computational domain of the Delft3D-Flow hydrodynamic model, highlighting key sites (e.g., Kratie, Kompong Luong, and Prek Kdam). (c) The canal network between Kratie and the Tonle Sap-Mekong confluence incorporated in the model to represent

floodplain connectivity and exchange via the Tonle Sap River. Note: The Phnom Penh Port station is shown for reference and is used only for river cross-section validation (Fig. S1), not for the flow regime analysis.

2.2 Station selection

To capture spatially representative changes in flow regime across the Mekong, this study analyzes data from eight mainstream hydrological stations, ranging from Chiang Saen in northern Thailand (representing upper-basin inflow conditions) to Kratie in Cambodia (located upstream of the Tonle Sap confluence) (Fig. 1a).

Additionally, we incorporated data from two supplementary stations for hydrodynamic validation and discharge lag-adjustment: Prek Kdam, situated on the Tonle Sap River and Kompong Luong, a monitoring station within the Tonle Sap Lake (Fig. 1b). These stations were used to validate the Delft3D-Flow hydrodynamic model, which was calibrated to simulate flood inundation and reverse flow in the floodplain (see detailed information in Sect. 2.5.2).

2.3 Period classification

To capture the evolving anthropogenic impacts on the Mekong River system, we classified the historical record into three distinct hydrological periods: pre-dam (1976-1991), transition (1992-2009), and post-dam (2010-2024). The pre-dam period represents the baseline hydrological state, dominated by natural monsoonal variability and minimal human interference, with no major mainstream dams constructed during this time (Chua et al., 2022; Morovati et al., 2024b). The transition period marks the onset of large-scale regulation, with the construction of the Manwan (1992), Dachaoshan (2003), and Jinghong (2009) dams along the Lancang mainstream, alongside expansion of tributary dam networks across the lower Mekong basin (Morovati et al., 2024b). This phase also saw the emergence of relatively large-scale sand mining in Cambodia, with estimated extraction volumes reaching ~13.5 Mt yr^{-1} (United Nations, 2017; Chua et al., 2022). The post-dam period is characterized by intensified regulation, marked by the commissioning of two mega-dams–Xiaowan (2010) and Nuozhadu (2014), which together increased upstream storage capacity by over 36,000 Mm^3. This period also featured widespread dam construction in tributaries and the expansion of irrigation infrastructure (Morovati et al., 2024b). Concurrently, sand mining intensified sharply, with annual extraction volumes in Cambodia surpassing 59 Mt yr^{-1}, significantly reshaping riverbed morphology and hydraulics near the Mekong-Tonle Sap confluence (Hackney et al., 2021, 2025; Quan et al., 2025). These compounding hydrological and morphological alterations are likely to affect not only flow magnitude and timing but also threshold-dependent dynamics such as the initiation and cessation of reverse flow into Tonle Sap Lake.

2.4 Data sources and preprocessing

Daily discharge data spanning 1976-2024 were obtained from the MRC Data Portal (https://portal.mrcmekong.org/home). Quality checks were applied to remove duplicates, missing dates, and outliers. For each station, we constructed a continuous daily time series (n=17,898 days) and identified missing dates by comparison with the full daily index. Missing records were rare (0-9 days per station; maximum at Kratie: 9 days = 0.050% of the record), totalling 18 missing station-day entries across

eight stations (0.0126% of all station-day values). Isolated one-day gaps were filled by linear interpolation between adjacent days. The only multi-day gap (Kratie, 2003-01-24 to 2003-01-28) was infilled using the upstream station discharge at Stung Treng plus intervening tributary inflow between Stung Treng and Kratie derived from the THREW model (Table. S1 in the Supplement).

To assess dam-induced changes in flow, simulated daily discharge without dam influence for the post-dam period (2010-2024) was obtained from validated THREW hydrological simulations (see Sect. 2.5.1). Except for this case, our analyses reflect the compounded impacts of dam regulation and climate variability, and we do not explicitly disentangle their relative contributions (Fig. 2d-f). Accordingly, measured post-dam flows inherently capture both influences, and our results should be interpreted within this combined context.

Water level datasets, including both daily and sub-daily (15-minute interval) records, were also accessed through the MRC portal. Sub-daily water level data were available from 2018 onwards, and corresponding analyses were limited to this sub-period. For hydrodynamic analyses of the Tonle Sap system, additional time series of lake water levels, reverse flow periods, and discharge were acquired from the MRC and Procedures for the Maintenance of Flows on the Mainstream (PMFM) online platform (https://pmfm.mrcmekong.org/monitoring/6b/).

The THREW hydrological simulations were forced using station-based meteorological observations from MRC and the China Meteorological Administration (CMA). Daily potential evapotranspiration was computed using the Penman-Monteith approach based on station meteorological variables (including temperature, wind speed, humidity, and radiation/sunshine duration; Fig. S3). Land-surface datasets used for parameterization included soil properties from the FAO global soil database (~10 km) and MODIS-based surface-condition products (NDVI, LAI, and snow cover; 500 m, 16-day), processed following Zhang et al. (2023) and aggregated to model units as described in Sect. 2.5.1.

To support hydrodynamic simulation of the lower Mekong-Tonle Sap-Delta system, we utilized riverbed cross-sectional bathymetry for two years (1999 and 2018, 250 measured cross sections), obtained from MRC and other hydrological agencies. These datasets were used as bathymetric inputs for the Delft3D-Flow model (see Sect. 2.5.2). For the pre-dam and transition periods (1976-2009), the 1999 cross sections were applied, reflecting minimal sand mining-induced incision during this time. For the post-dam period (2010-2024), the more incised 2018 dataset was used to represent altered channel morphology due to intensified sand extraction. Adjacent measured transects are irregularly spaced along the thalweg (300 to 3,000 m). To derive a hydraulically consistent continuous bathymetry from these discrete transects, we reconstructed intermediate cross-sections in a curvilinear reference frame defined by the river centreline (chainage) and signed cross-channel distance. For each transect, we fit a third-order polynomial bed profile and extracted left- and right-bank elevations; the resulting profile parameters were interpolated along chainage using monotone piecewise-cubic interpolation (PCHIP). Between each pair of measured transects, we generated 30-200 virtual cross-sections (~100 points per transect), enforcing (i) bank anchoring at the interpolated bank elevations and (ii) envelope clipping that constrains interior bed elevations to the min-max range of the bracketing surveyed transects. We also applied a smoothness constraint to suppress unrealistic lateral jumps in the thalweg. The measured and virtual cross-sections were then mapped onto the Delft3D curvilinear grid using

Delft3D-QUICKIN, which applies triangular interpolation and internal diffusion to generate a continuous DEM at each grid-node corner (see Sect. 2 in the Supplement for more details).

Additionally, FABDEM elevation data (Forest and Buildings removed Copernicus DEM) with 30-meter spatial resolution were incorporated to define floodplain topography and overbank areas beyond the main river channels. For the hydrodynamic simulations, observed daily discharge at Kratie obtained from MRC was prescribed as the upstream inflow boundary, while tributary inflows to the Mekong mainstream and the Tonle Sap system were specified using THREW-simulated daily discharge at tributary outlets (see Sects. 2.5.1 and 2.5.2).

2.5 Methods

2.5.1 Hydrological model

Due to the absence of measured daily discharge data for tributaries discharging into the Mekong mainstream and the Tonle Sap Lake (see Fig. 1b), we employed the Tsinghua Representative Elementary Watershed (THREW) model to simulate tributary inflows. In parallel, to generate a baseline scenario for the post-dam period (2010-2024) that is unimpacted by dam operations, we also applied the THREW model to estimate naturalized discharge along the Mekong mainstream. The THREW model is a spatially distributed, physically based hydrological model designed to operate at the scale of Representative Elementary Watersheds (REWs), which preserve physical realism while ensuring computational efficiency. The model has been extensively validated in large transboundary basins, including the Mekong (Morovati et al., 2021, 2023, 2024b; Zhang et al., 2023) (see Sect. 3 in the Supplement for more information).

The entire Mekong River basin was discretized into 651 REWs, allowing spatial representation of diverse hydrological processes across climatic and topographic gradients (Fig. S2 in the Supplement). The THREW hydrological simulations were driven by station-based precipitation and meteorological observations from the MRC and the China Meteorological Administration (CMA). Precipitation was obtained from a basin-wide gauge network (105 stations) and air temperature from 35 stations (Fig. S3 in the Supplement). Daily potential evapotranspiration was computed using the Penman-Monteith method based on station meteorological variables (including temperature, wind speed, humidity, and radiation/sunshine duration). Soil properties were taken from the FAO global soil database (10 km). Vegetation and surface-condition inputs (NDVI, LAI, and snow cover) were derived from MODIS products (500 m, 16-day) following Zhang et al. (2023). Site-based meteorological inputs (e.g., precipitation, temperature) were spatially allocated to REWs using the Thiessen polygon method (Fig. S3 in the Supplement). For gridded datasets such as Leaf Area Index (LAI) and Normalized Difference Vegetation Index (NDVI), spatial intersection analyses were performed to determine the weighted contributions of raster cells falling within each REW. The weighted averages of these variables were then assigned as REW-scale inputs.

Model calibration was conducted using an automatic parallel computation framework that optimizes hydrological parameters across multiple REWs simultaneously (Nan et al., 2021) (Table S2 in the Supplement). This enabled efficient exploration of the parameter space while maintaining consistency with observed discharge data at available gauging stations. The THREW

model was calibrated for 2000-2009 and validated for 1980-1999 using observed discharge at available gauging stations; detailed performance metrics are provided in the Supplement. The THREW model was used to simulate daily discharge for all tributaries flowing into the Mekong and the Tonle Sap Lake, providing critical boundary conditions for the hydrodynamic simulations described in Sect. 2.5.2.

2.5.2 Hydrodynamic model

To simulate flow propagation and water surface dynamics across the lower Mekong River-Tonle Sap-Delta system, we developed a three-dimensional, grid-based hydrodynamic model using Delft3D-Flow (Deltares, 2014). The model domain spans from the Kratie gauging station in Cambodia to approximately 80 km offshore, encompassing the Tonle Sap Lake and River, the Cambodian floodplain, and the Vietnamese delta (Fig. 1b).

Given the meandering nature of the Mekong River and its distributaries, we adopted a spherical coordinate system to minimize discretization errors associated with angular distortion and to ensure the accurate representation of curved channel boundaries. The model employed the cyclic method for advection and the k–ε turbulence closure scheme, which is well-suited for resolving complex three-dimensional flow structures in fluvial-estuarine systems (Morovati et al., 2023; Wu et al., 2024).

The Kratie station served as the primary upstream inflow boundary, where we imposed time-series discharge based on observed daily data. In addition, discharge time series for all major tributaries entering the Mekong mainstream or the Tonle Sap system were also defined as inlet boundaries. These were derived from a calibrated and validated physically based hydrological model (see Sect. 2.5.1). Inflow boundaries were assigned to a vertically uniform profile. The downstream open boundary was defined approximately 80 km offshore, where tidal forcing was applied using nine dominant tidal constituents (M2, S2, K1, O1, N2, P2, K2, O2, and Q4). This tidal boundary ensured a realistic representation of tidal propagation and backwater effects from the sea into the Mekong estuarine system. The model was run with a 1-minute time step.

The horizontal grid resolution varied from 20 m in river channels and Tonle Sap tributaries to 250 m in floodplains and offshore areas. A finer resolution was employed within the river network and lake system to accurately capture channel morphology and water level gradients, both of which are critical for simulating reverse flow phenomena and calculating travel times. A one-year warm-up period was considered for simulations. The first simulation year was treated as a spin-up period and excluded from the analysis. Over the subsequent period, the model reproduces observed daily water levels and reverse flow characteristics with high skill at Prek Kdam and Kompong Luong–stations used to validate the hydrodynamic model (NSE > 0.92; Supplement Sect. 4)–indicating limited sensitivity to initial conditions and that a one-year warm-up is sufficient for this application.

Around the Tonle Sap-Mekong confluence, many natural and artificial canals interact with the Mekong and Tonle Sap River, influencing overland flow exchange during both reverse and non-reverse flow periods. These lateral exchanges, which can exceed 5 $km^3\ yr^{-1}$ (Kummu et al., 2014; Morovati et al., 2023), were fully incorporated into the hydrodynamic model. To represent these flows, we extracted canal networks using a machine learning-based remote sensing model developed by Zhao

et al. (2025), supplemented by manual digitization from high-resolution satellite imagery (Fig. 1c). This enabled a more realistic representation of hydraulic connectivity between rivers, floodplains, and the lake. More details can be found in Zhao et al. (2025).

Bathymetry was derived from the surveyed cross-sections (spacing 300-3,000 m) using the interpolation procedure described in Sect. 2.4 and mapped to the Delft3D curvilinear grid with Delft3D-QUICKIN (triangular interpolation with internal diffusion). Interpolation performance, assessed via leave-one-section-out cross-validation and independent-transect comparisons, achieved an RMSE of 0.46 m and a median absolute error of 0.37 m.

2.5.3 Response time model

To quantify the time lag between discharge at Kratie and its impact at the Mekong-Tonle Sap confluence, we developed a response time model embedded within the hydrodynamic framework described in Sect. 2.5.2.

The concept of response time, also referred to as water age, reflects the transit time required for water parcels to travel from a specified upstream point to a downstream target location (Morovati et al., 2024b). It characterizes the average residence time of water traveling from the Kratie station (inlet boundary) to the Mekong-Tonle Sap confluence. This metric inherently accounts for spatial heterogeneity in flow velocity and channel morphology and thus provides a physically meaningful measure of hydrodynamic connectivity (Wu et al., 2024).

We implemented a 3D response time (age) model using an Eulerian framework, following the methodology of Shi et al. (2023). Within this framework, a virtual passive tracer–assumed to be neutrally buoyant and non-reactive–was continuously injected at the inlet boundary (Kratie). This tracer does not alter water density or momentum fields and is solely used to track water mass movements (Morovati et al., 2024b). The response time (a) at a given location is defined as the average elapsed time since the tracer particles first exited the inlet, weighted by their mass.

The evolution of tracer concentration (C) and age concentration (α) is governed by coupled advection-diffusion equations derived from the principle of mass conservation:

$$\frac{\partial C}{\partial t} + (\nabla \cdot \mathrm{u})C + \frac{\partial wC}{\partial z} = \nabla(D_h \cdot \nabla)C + \frac{\partial}{\partial z}\left(D_v \frac{\partial C}{\partial z}\right) \quad (1)$$

$$\frac{\partial \alpha}{\partial t} + (\nabla \cdot \mathrm{u})C + \frac{\partial w\alpha}{\partial z} = \nabla(D_h \cdot \nabla)\alpha + \frac{\partial}{\partial z}\left(D_v \frac{\partial \alpha}{\partial z}\right) + C \quad (2)$$

$$a = \frac{\alpha}{C} \quad (3)$$

Here, C is the tracer concentration, α is the age concentration (i.e., the product of tracer concentration and residence time), D is the turbulent diffusivity tensor, u is the velocity vector obtained from the hydrodynamic model, and a is the final computed response time at each model grid cell. ∇ is the Hamiltonian operator.

2.5.4 Hurst exponent: Long-term memory of flow

To quantify the persistence or memory of discharge fluctuations over time, we computed the Hurst exponent (H) using the Rescaled Range (R/S) method, a widely used method in hydrological studies (Khan et al., 2025). The Hurst exponent captures the degree of autocorrelation and long-range dependence in time series, with H > 0.5 indicating persistence, $H < 0.5$ signifying anti-persistence, and H~0.5 denoting stochastic behavior. The discharge time series Q_t is divided into multiple non-overlapping segments of equal length n, spanning a wide range of scales. For each segment, the series is mean-centered and transformed into a cumulative deviation series (Eq. 4), where $\bar{Q}$ is the mean discharge of the segment.

$$Y(t) = \sum_{i=1}^{t}(Q_i - \bar{Q}) \quad (4)$$

The rescaled range R/S is then calculated for each segment (Eq. 5):

$$R(n) = \max\big(Y(t)\big) - \min\big(Y(t)\big), \quad S(n) = \sqrt{\frac{1}{n}\sum_{i=1}^{n}(Q_i - \bar{Q})} \quad (5)$$

Then, the average R/S is plotted as a function of window size n in log-log space (Eq. 6)

$$\log(R/S) = H \times \log(n) + C \quad (6)$$

The slope of the best-fit line yields the Hurst exponent $H \in (0, 1)$. This method was implemented using the Hurst Python Package.

2.5.5 Richards-Baker Flashiness Index (RBI): High-Frequency Variability

The Richards-Baker Flashiness Index (RBI) was used to evaluate the short-term variability and flow "flashiness" of the discharge series and sub-daily water levels. It is a measure of how quickly and how streamflow rises and falls in response to watershed input (Gannon et al., 2022). RBI is calculated as:

$$RBI = \frac{\sum_{i=2}^{n}|Q_i - Q_{i-1}|}{\sum_{i=1}^{n} Q_i} \quad (7)$$

where Q_i is the daily discharge on day i, and n is the number of valid observations. RBI values range from 0 (completely stable flow) to >1 (highly variable, flashy flows). This metric captures the magnitude and frequency of day-to-day discharge changes, allowing assessment of how dam regulation has attenuated or enhanced hydrograph variability.

2.5.6 Coefficient of Variation (CV): Interannual discharge variability

To assess changes in relative flow variability across the basin, we computed CV for each station and time period as (Blöschl and Sivapalan, 1997; Li et al., 2025):

$$CV = \frac{\sigma Q}{\mu Q} \quad (8)$$

where σ_Q and μ_Q denote the standard deviation and mean of daily discharge, respectively. This dimensionless index provides a standardized measure of variability that facilitates comparisons between stations with differing flow magnitudes.

2.5.7 Sub-daily water-level variability metrics

Sub-daily water level variability was quantified using three complementary metrics derived from 15-min water-level records (available from 2018 onward). For each day d, amplitude (A) was defined as the daily range of sub-daily water levels (WL):

$$A_d = WL_{max,d} - WL_{min,d} \quad (9)$$

Monthly amplitude was computed as the mean of A_d over all days in the month. Sub-daily flashiness was computed using the Richards-Baker formulation, substituting water level for discharge and applying the calculation within each calendar month:

$$RBI_{WL} = \frac{\sum_{i=2}^{n} |WL_i - WL_{i-1}|}{\sum_{i=1}^{n} WL_i} \quad (10)$$

where WL_i denotes consecutive 15-min observations within the month, and n is the number of valid records. This yields a dimensionless index of intramonth sub-daily variability. Peak count was defined as the number of positive hourly water level rises exceeding a threshold of 0.05 m h^{-1} (i.e., 5 cm h^{-1}), following the rate-of-change guidance referenced by the MRC (MRC, 2020). The 15-min series was resampled to hourly water levels. Daily peak count was reported as events per day and aggregated to monthly values by averaging across days.

3 Results

3.1 Model validation

The performance of the THREW and Delft3D-Flow models was evaluated across multiple hydrological stations. Both models demonstrated high accuracy in reproducing discharge and water level time series, with Nash-Sutcliffe Efficiency (NSE) values exceeding 0.88. Detailed validation results and station-specific performance metrics are provided in the Supplement, Sects. 3 and 4.

3.2. Multi-scale streamflow alterations under dam regulation and climate change

Six rose diagrams (Fig. 2a-f) summarize the spatiotemporal evolution of discharge dynamics across eight mainstream stations from Chiang Saen to Kratie. The top row shows observed changes across three hydrological periods, while the bottom row compares measured conditions with a no-dam counterfactual for the post-dam era (2010-2024). All metrics are derived from the daily discharge series. The no-dam daily discharge series for 2010-2024 is taken from the THREW model simulations.

Flow memory (Hurst exponent, H) captures long-range persistence in daily discharge variability (Fig. 2a). H is highest upstream and generally decreases downstream across all periods, but the upstream-downstream contrast strengthens in the post-dam era. For example, H increases at Chiang Saen from ~0.58 (pre-dam) to ~0.69 (post-dam), whereas Kratie decreases from ~0.53 to ~0.47. The post-dam comparison between observations and no-dam simulations confirms that the increase in persistence is concentrated in the regulated upper reach: measured H exceeds the no-dam case at upstream stations (e.g., Chiang Saen: 0.69 vs 0.56), while differences are small and can reverse in the lower basin (e.g., Kratie: 0.47 vs 0.48) (Fig.

2d). This pattern is consistent with reservoir operations strengthening persistence upstream, while monsoon-driven runoff contributions from downstream tributaries and adjacent floodplains, which become increasingly important in the lower basin modulate (and may offset) that signal.

Daily flashiness (RBI) quantifies day-to-day discharge fluctuations (Fig. 2b). RBI is consistently largest at the upstream station (Chiang Saen) and decreases toward the mid-lower basin in all periods, with values on the order of ~0.03–0.07. Across periods, RBI increases modestly at the upstream stations (e.g., Chiang Saen: ~0.060 pre-dam to ~0.065 post-dam), but declines at downstream stations (e.g., Kratie: ~0.043 to ~0.036), indicating spatially heterogeneous changes in day-to-day variability (Fig. 2b). In the post-dam comparison between observations and the no-dam simulation, measured RBI is higher than the no-dam counterfactual at all stations, with the strongest relative increase upstream (e.g., Chiang Saen: 0.065 vs 0.039; Chiang Khan: 0.050 vs 0.033) (Fig. 2e). This suggests that, at the daily scale, regulation is associated with enhanced day-to-day fluctuations relative to the counterfactual hydrograph, while the magnitude of this effect weakens downstream.

Amplitude variability (coefficient of variation, CV) reflects the combined seasonal and interannual variability of daily discharge (Fig. 2c). CV is high in the pre-dam and transition periods and tends to increase downstream, but it declines substantially in the post-dam era at upstream sites (e.g., Chiang Saen: ~0.77 pre-dam to ~0.52 post-dam; Chiang Khan: ~0.85 to ~0.71), consistent with dampened wet-season peaks and enhanced dry-season flows under reservoir regulation. The post-dam comparison between observations and no-dam simulations supports this interpretation in the upper reach (e.g., Chiang Saen: 0.52 vs 0.68; Chiang Khan: 0.71 vs 0.81; Nong Khai: 0.74 vs 0.81), whereas differences are small downstream (e.g., Mukdahan-Kratie) (Fig. 2f), consistent with attenuation of the regulation signal and increasing influence of tributary inflows and floodplain dynamics in the lower basin.

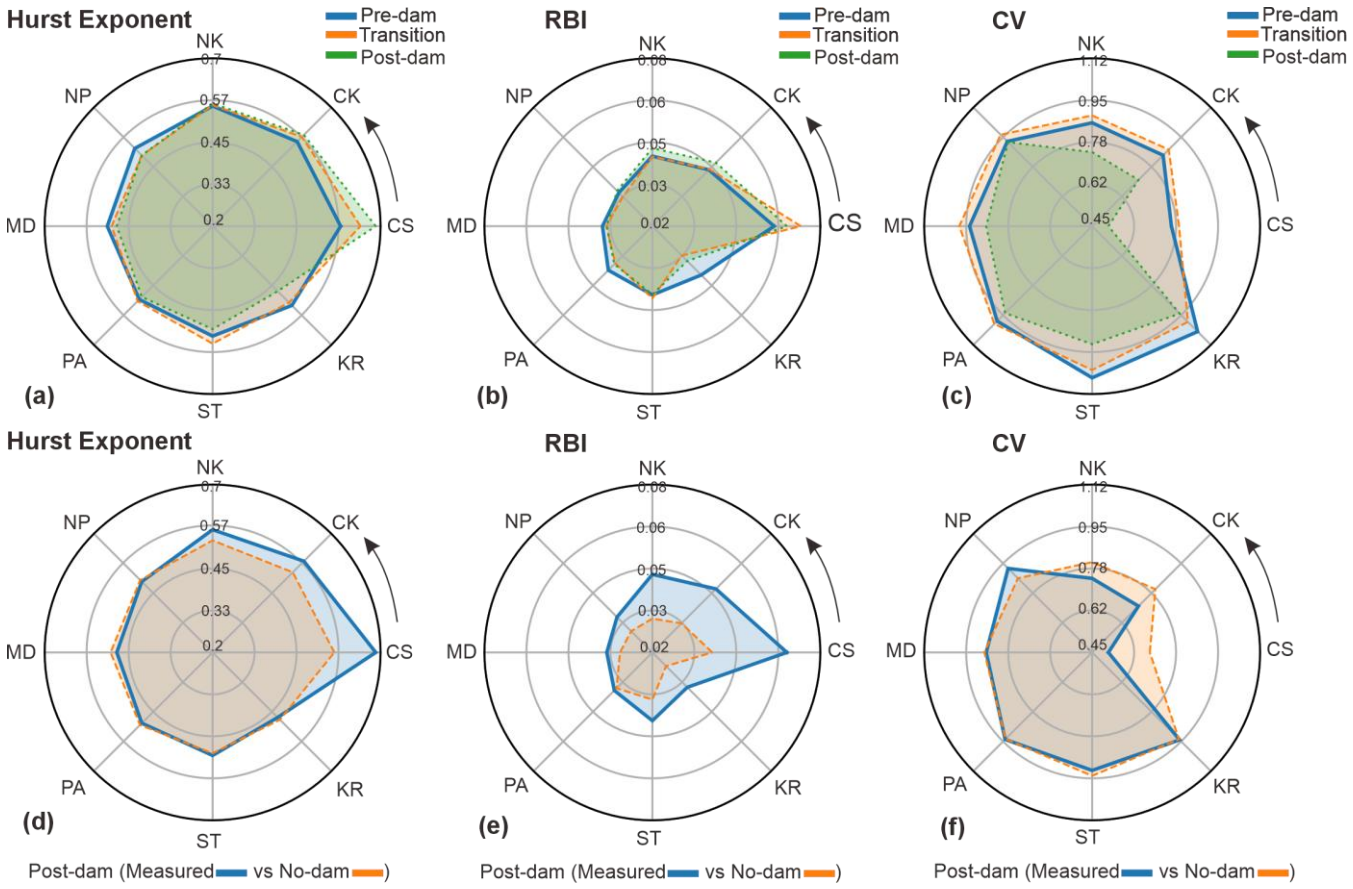


Figure 2. Spatial patterns of streamflow memory, flashiness, and variability along the Mekong mainstream under observed and no-dam conditions. Six rose diagrams summarize hydrological dynamics at eight mainstream stations from Chiang Saen to Kratie. The top row (a-c) compares three hydrological periods–pre-dam (1976-1991), transition (1992-2009), and post-dam (2010-2024)–for (a) the Hurst exponent (H), (b) the Richards-Baker flashiness index (RBI), and (c) the coefficient of variation (CV). The bottom row (d-f) compares post-dam conditions under observed (measured) and a no-dam counterfactual simulated with the THREW hydrological model. Curved arrow indicates the station sequence from upstream to downstream within each panel. Station abbreviations are CS, CK, NK, NP, MD, PA, ST, and KR for Chiang Saen, Chiang Khan, Nong Khai, Nakhon Phanom, Mukdahan, Pakse, Stung Treng, and Kratie, respectively.

3.3 Spatial patterns of sub-daily flow variability

Figure 3 illustrates sub-daily water level dynamics at three representative mainstream stations–Chiang Saen (CS; Fig. 3a-c), Mukdahan (MD; Fig. 3d-f), and Kratie (KR; Fig. 3g-i)–using three complementary metrics: (i) amplitude, defined as the intraday water level range (daily max-min; m), (ii) flashiness (RBI) computed from sub-daily water level changes, and (iii)

peak count, defined as the mean number of hourly water-level rises ≥ 5 cm h^{-1} per day. The 5 cm h^{-1} threshold follows MRC guidance as a rate-of-change level above which ecological impacts may increase (MRC, 2020).

Amplitude exhibits a consistent wet-season intensification across the three stations, but with station-specific magnitude and timing (Fig. 3a, d, g). At CS, amplitudes increase markedly during the wet season (typically June–September), with notable high-variability months including July 2021 (~0.48 m) and August-September 2024 (~0.40-0.46 m), while many dry-season months remain comparatively muted. At MD, amplitudes are generally lower and more moderate, but still strengthen during wet-season months (commonly July-September), reaching ~0.2-0.3 m in several years. At KR, the wet-season signal is more pronounced and can extend into late wet season, culminating in a strong event in September 2019 (~0.77 m). The corresponding matrices for the remaining stations (CK, NK, NP, PA, ST) show that larger amplitudes can occur at mid-reach stations in particular years/months (Supplementary Fig. S7), reinforcing that sub-daily variability is spatially heterogeneous and episodic.

Flashiness (RBI) broadly tracks the occurrence of rapid intraday changes but highlights the intermittency of short-lived fluctuation episodes (Fig. 3b, e, h). RBI at CS is generally low but displays distinct episodic enhancements, including a prominent increase in February 2022 (~0.004) and elevated wet-season values during months of higher amplitude (e.g., July 2021). At MD, RBI remains low for many months but includes isolated months with higher values (e.g., late 2019 and early 2021), indicating that rapid fluctuations can emerge intermittently even when typical conditions are relatively smooth. At KR, RBI is usually low but increases during months with stronger wet-season dynamics, including September 2019 (~0.0017) and June 2020 (~0.0017), consistent with periods of intensified intraday variability. Supplementary Fig. S7 indicates that some mid-mainstream stations can reach substantially higher RBI in specific wet-season months, underscoring the episodic nature of flashiness along the reach.

The peak count metric isolates where rapid hourly rises are frequent and shows that exceedances of the 5 cm h^{-1} threshold are seasonally concentrated and event-driven rather than pervasive (Fig. 3c, f, i). At CS, peak counts are zero in many months but rise sharply during certain wet-season months, including July 2021 (~2.0 events day^{-1}) and August-September 2024 (~1.3-1.4 events day^{-1}). At MD, exceedances are rarer overall and typically confined to isolated wet-season months (e.g., July 2018 and August 2020), indicating fewer frequent rapid-rise events than at CS and KR. At KR, exceedances can be both larger and more frequent in the wet season, with a major episode in September 2019 (~4.4 events day^{-1}) and elevated activity in June 2020 (~2.6 events day^{-1}). Across the full station set (Supplementary Fig. S7), the most frequent exceedances occur at selected mid-reach stations during particular wet season months, highlighting strong spatial clustering of rapid water-level rises.

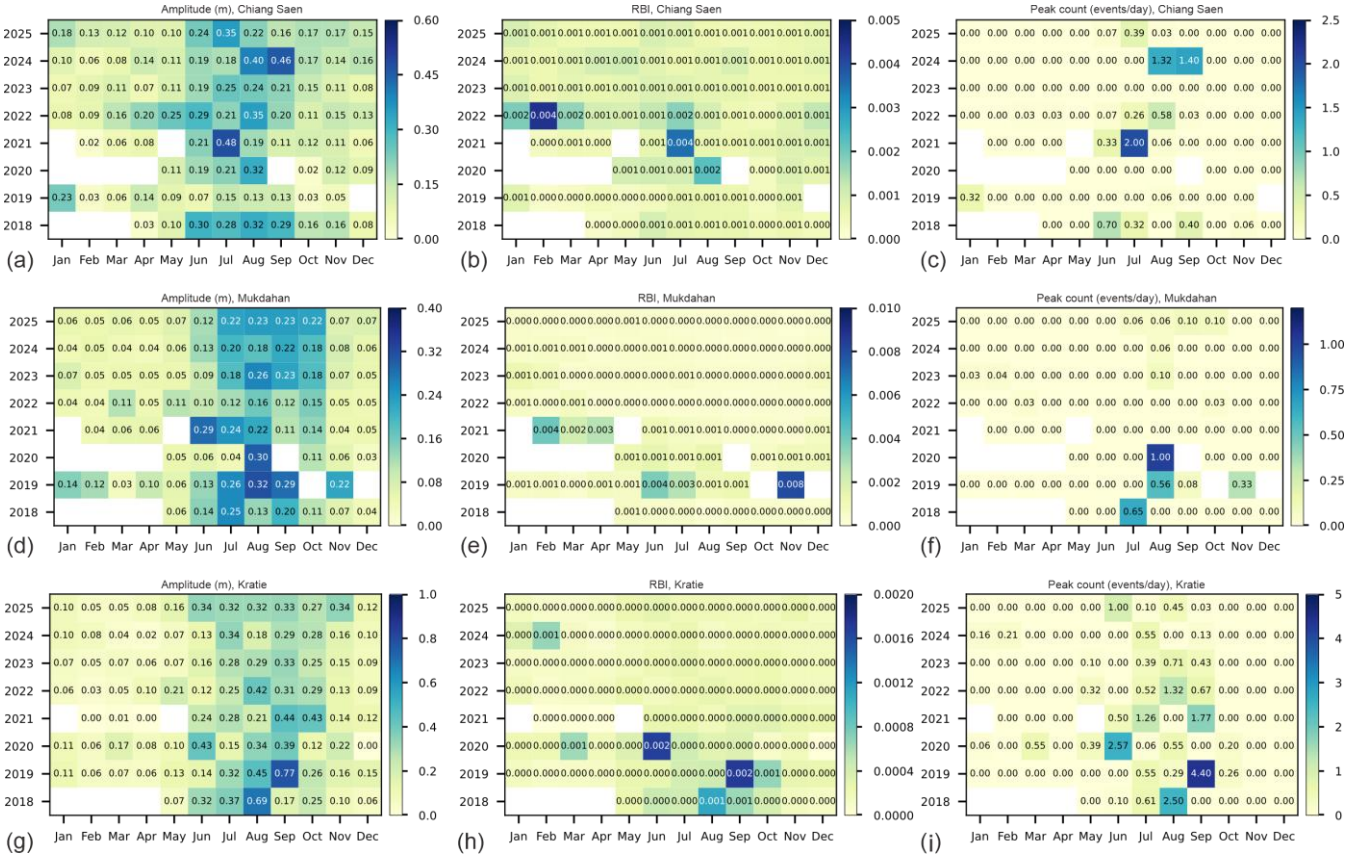


Figure 3. Sub-daily water level variability at three representative Mekong mainstream stations (2018-2025). Sub-daily dynamics are quantified from 15-min water level observations using three complementary metrics: intraday amplitude (daily max-min water level, m), flashiness (Richards-Baker Index, RBI, computed from sub-daily water-level changes), and peak count (mean number of hourly water-level rises ≥ 5 cm h^{-1} per day). Panels (a-c) show Chiang Saen (CS); panels (d-f) show Mukdahan (MD); and panels (g-i) show Kratie (KR). Each panel displays monthly values by year; numbers denote the metric value for that station-month. Blank cells indicate months without available 15-min water level records. Results for the remaining mainstream stations (Chiang Khan, Nong Khai, Nakhon Phanom, Pakse, and Stung Treng) are shown in Supplement, Fig. S7

3.4 Changes in annual discharge extremes and their timing

A pronounced reduction in annual peak discharge is evident at several stations following upstream dam development (Fig. 4a). At Chiang Saen, which reflects transboundary inflow from the Lancang cascade, the median peak flow declined by ~ 40%, from ~10,850 m^3 s^{-1} in the pre-dam period to ~6,493 m^3 s^{-1} in the post-dam era. Similar, though less pronounced, reductions in median peak discharge are observed at Chiang Khan and Nong Khai, where values declined by approximately 11.4% and 8.4%, respectively, from the pre-dam to post-dam period. These trends reflect attenuated flood pulses

downstream of the Chinese cascade and possibly early regulatory effects from tributary inflows. In contrast, Nakhon Phanom exhibited a 9.6% increase in peak discharge, suggesting localized hydrological intensification, potentially influenced by regional rainfall variability or unregulated tributary contributions. At Kratie–a hydrologically strategic station controlling the Mekong inflow to the Tonle Sap River and lake during the wet season months–the median annual peak discharge declined from ~ 38,300 $m^3 s^{-1}$ in the pre-dam period to 34,700 $m^3 s^{-1}$ in the post-dam period, representing a 9.4% reduction.

Conversely, annual minimum discharges exhibit a consistent increasing trend across all stations, particularly during the post-dam period (Fig. 4c). At Chiang Saen, the median minimum discharge rose from approximately 748 $m^3 s^{-1}$ in the pre-dam period to 997 $m^3 s^{-1}$ in the post-dam period–an increase of 33.3%, reflecting enhanced baseflow likely sustained by regulated dam releases. This upward trend is even more pronounced downstream. At Stung Treng, minimum flow increased from 1,565 $m^3 s^{-1}$ to 2,820 $m^3 s^{-1}$, a remarkable 80.2% rise. Most notably, at Kratie, minimum discharge surged from 1,326 $m^3 s^{-1}$ in the pre-dam period to 2,880 $m^3 s^{-1}$ in the post-dam period, marking an increase of 117.2%. These substantial increases in dry-season flow highlight the transformative impact of upstream tributary and mainstream reservoir storages and regulated releases on the seasonal amplitude of Mekong River discharge, potentially compressing the natural flood pulse regime and altering the hydro-ecological dynamics of the floodplain and Tonle Sap system.

In the pre-dam period, peak flows generally occurred between early August and early September across all stations, aligned with the core of the monsoon season (Fig. 4b). However, dam regulation and reservoir operations have systematically delayed the timing of peak flows in the post-dam period. Peak flow timing at most stations has shifted by approximately 10-20 days later. At Kratie, the median day of peak flow occurred around late August, whereas in the post-dam period, this timing has shifted to approximately mid-September.

The timing of annual minimum flows has consistently advanced across all stations along the Mekong mainstream (Fig. 4d). At Kratie, for example, the timing of median minimum discharge shifted from early April (April 10) to mid-March in the post-dam period, an advancement of nearly a month. Similar shifts are observed throughout the basin, with Chiang Saen advancing from March 25 to March 2, Chiang Khan from April 9 to March 14, Stung Treng from April 9 to March 11, and from April 10 to March 12. These 2-4-week advancements in low-flow timing suggest a system-wide shift in hydrological seasonality, likely driven by altered monsoon onset patterns and the compounded influence of reservoir discharge strategies in both the upper and lower Mekong basin.

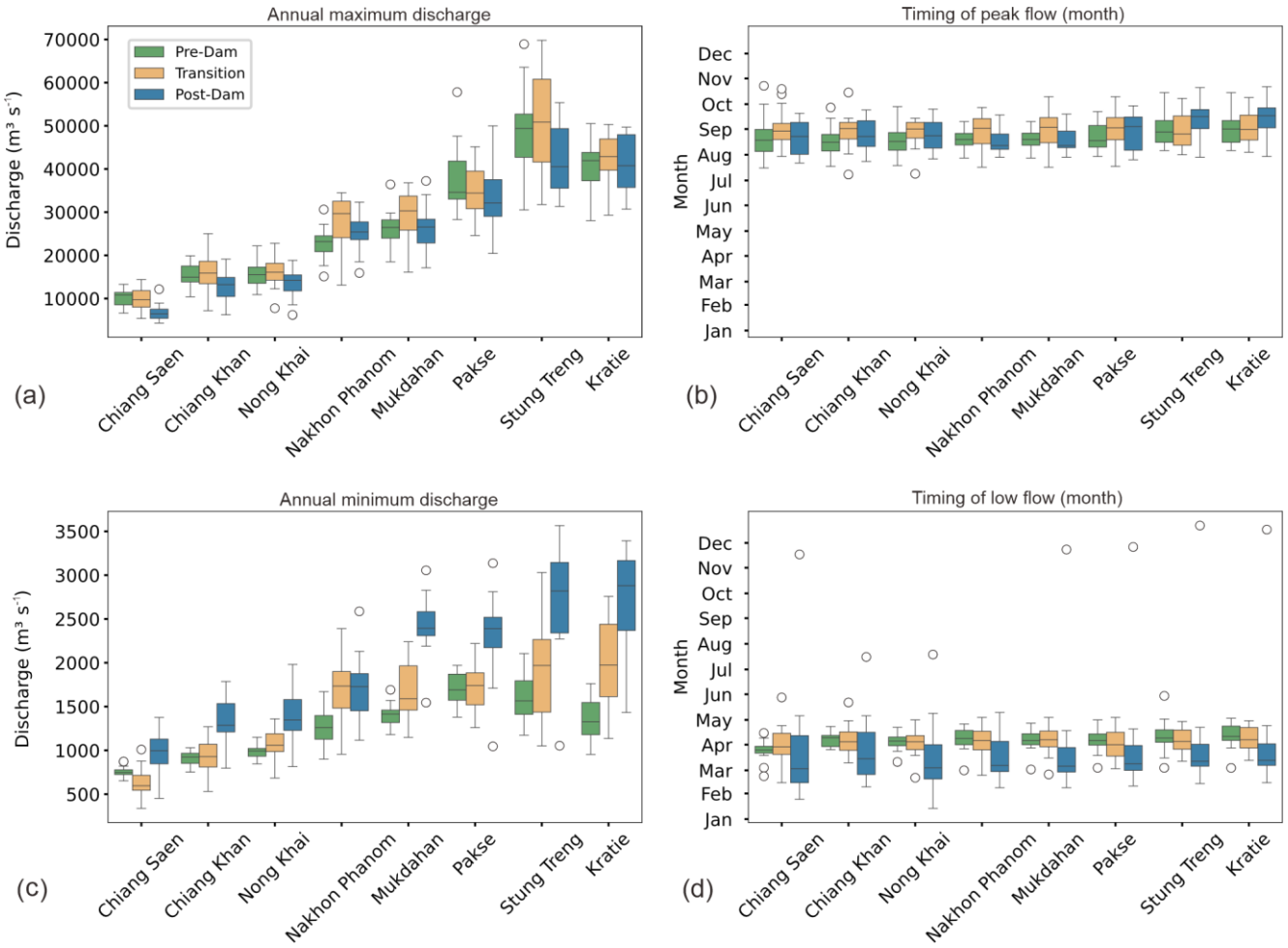


Figure 4. Alterations in annual discharge extremes and their timing across the Mekong mainstream. Boxplots show the spatial and temporal evolution of (a) annual maximum daily discharge, (b) timing of annual maximum discharge, (c) annual minimum daily discharge, and (d) timing of annual minimum discharge.

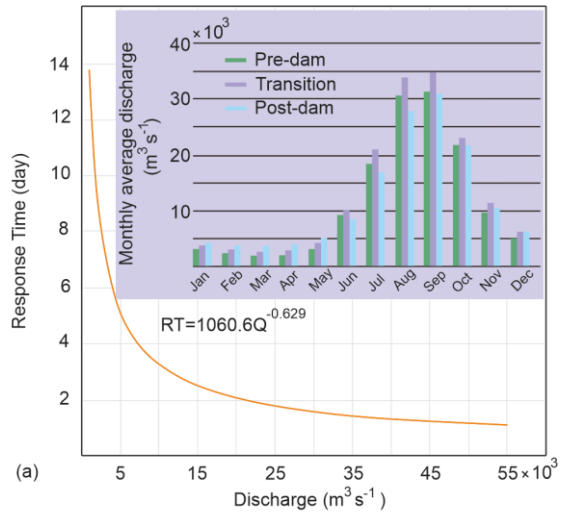
3.5 Lag-adjusted Kratie discharge thresholds for reverse flow onset and cessation

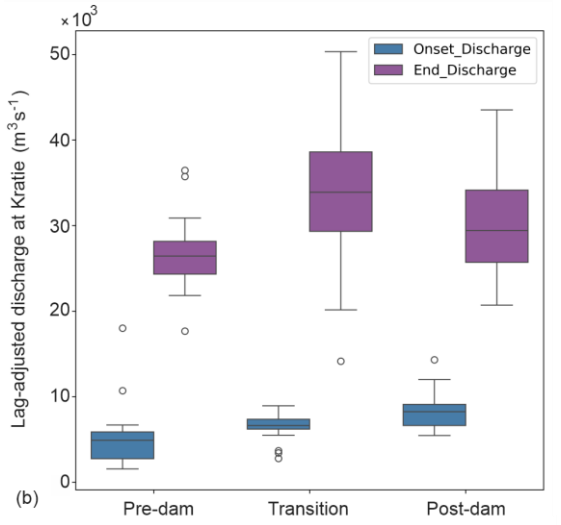
Here, "threshold" denotes the lag-adjusted Kratie discharge associated with the observed onset and cessation of reverse flow, used as an operationally interpretable proxy for hydraulic conditions at the confluence. It is therefore influenced by local stage-discharge relations (including incision effects) and by the timing-dependent head difference between the mainstream and the lake, rather than representing a fixed geometric constant. Figure 5a shows (i) the nonlinear discharge-travel time relationship between Kratie and the Mekong-Tonle Sap confluence and (ii) period-specific differences in the monthly discharge regime. The fitted power-law relationship ($RT = 1060.6 \times Q^{-0.629}$) indicates that travel time decreases rapidly with increasing discharge; during the wet season's peak discharges (June-November), flows at Kratie typically reach the

confluence within ~1-3 days. The inset monthly hydrograph further indicates that the post-dam period exhibits a more peaked seasonal pattern, with reduced early wet season discharge (June-July) and a more abrupt rise toward the seasonal maximum. September remains the peak month across all periods.

Figure 5b presents the lag-adjusted discharge thresholds at Kratie associated with the onset (rising limb) and cessation (recession limb) of reverse flow into the lake. In the pre-dam period (1976-1991), reverse flow typically initiated when discharge exceeded ~3,000 $m^3 s^{-1}$ and ceased when discharge declined to ~28,000 $m^3 s^{-1}$. In the post-dam period (2010-2024), the onset discharge increased by 130% to ~7,000 $m^3 s^{-1}$, while reverse flow ceased when discharges fell to ~34,000 $m^3 s^{-1}$ (with some years surpassing 40,000 $m^3 s^{-1}$). This higher cessation value is consistent with earlier termination (late September rather than early October; Fig. 5c), when mainstream discharge is typically higher than during October, and with onset-cessation hysteresis driven by seasonal lake storage.

Figure 5c shows corresponding shifts in the timing of reverse flow. In the pre-dam period, the onset occurred in early June (median ~June 3-5). In the post-dam period, the onset shifted later by ~two weeks (median ~June 17). Conversely, cessation shifted earlier: whereas reverse flow typically ended in the first ten days of October during the pre-dam period, most post-dam years show end dates in late September. Together, these changes indicate a shorter reverse flow season in the post-dam period, reflecting both delayed onset and earlier cessation.


Response Time (day)
Discharge ($m^3 s^{-1}$)
Monthly average discharge ($m^3 s^{-1}$)
Pre-dam
Transition
Post-dam
Jan
Feb
Mar
Apr
May
Jun
Jul
Aug
Sep
Oct
Nov
Dec
RT=1060.6Q$^{-0.629}$
(a)


Lag-adjusted discharge at Kratie ($m^3 s^{-1}$)
Onset_Discharge
End_Discharge
Pre-dam
Transition
Post-dam
(b)

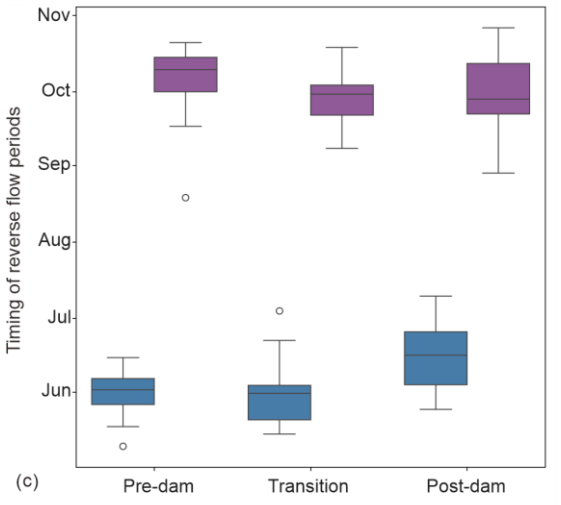

Timing of reverse flow periods
Nov
Oct
Sep
Aug
Jul
Jun
Pre-dam
Transition
Post-dam
(c)

Figure 5. (a) Estimated response times (days) for Kratie discharge to reach the Tonle Sap-Mekong confluence, overlaid with monthly average discharge at Kratie. (b) Lag-adjusted discharge thresholds at Kratie corresponding to the onset (left) and cessation (right) of reverse flow into the Tonle Sap Lake. (c) Timing of reverse flow onset (left) and cessation (right). Note that historical data on the Tonle Sap Lake's reverse flow period are available from 1997 onward (https://pmfm.mrcmekong.org/monitoring/6b/, last access: 16 July 2025). Consequently, we reconstructed reverse flow periods from 1976 to 1996 using a calibrated hydrodynamic model (see Sect. 4 in the Supplement)

4 Discussion

Large regulated monsoonal rivers can exhibit substantial changes in flow magnitude, yet our results indicate a deeper reorganization of Mekong dynamics: (i) dampening of the seasonal discharge envelope and altered early wet-season rise in the upper mainstream, alongside higher persistence and modest changes in day-to-day flashiness, (ii) altered spatiotemporal coherence along the mainstream, and (iii) a measurable shift in the hydraulic conditions governing Tonle Sap reverse flow. Collectively, these changes suggest a progressive departure from the natural flood pulse regime that underpins floodplain-lake connectivity and productivity in the lower Mekong-Tonle Sap system (e.g., Poff et al., 1997; Arias et al., 2012).

A central contribution of this study is the response-time (travel time) alignment between Kratie and the Mekong-Tonle Sap confluence, which enables onset/cessation thresholds to be interpreted as properties of the coupled river-lake system rather than as station-specific statistics. This framing also helps reconcile why downstream reach remains monsoon-driven even as upstream reaches show pronounced regulation: tributary inflows partly preserve seasonal variability downstream (Zhang et al., 2023; Morovati et al., 2024b), but they do not fully restore the early wet season rise and hydraulic gradients that historically initiated and sustained reverse flow.

4.1 Fragmentation across daily to sub-daily scales

The daily-metric synthesis indicates a regulation-driven reorganization rather than a uniform damping of variability. At Chiang Saen, persistence increases while discharge variability decreases (CV), consistent with seasonal redistribution and flood-peak attenuation, yet daily flashiness (RBI) increases modestly. This combination suggests that reservoirs smooth the seasonal envelope but can introduce shorter-term irregularity through storage-release sequencing and shifting tributary contributions. Downstream, tributary inflows partly preserve seasonal contrasts, while flashiness tends to decline toward Kratie, indicating that the regulation signal is expressed differently across timescales and along the longitudinal profile.

These changes are hydrologically meaningful because many floodplain processes respond to the rate of rise, onset timing, and duration of high water conditions (Poff et al. 1997; Bunn & Arthington, 2002; Lamberts & Koponen, 2008; Sabo et al., 2017), not only to seasonal totals. In the Tonle Sap system, timing-related controls influence floodplain access, the predictability of seasonal cues, and the window over which connectivity enables exchange of water, sediment, and nutrients (Baran and Myschowoda, 2009; Arias et al., 2014; MRC, 2017; Dudgeon, 2020). The observed sub-daily water level

variability further indicates that intraday fluctuations can represent an additional layer of disturbance. Although direct attribution is limited without operational release data, the patterns are consistent with hydropeaking behavior reported downstream of hydropower cascades (MRC, 2020), where rapid ramping can impose ecological stress through repeated short-duration rises and falls (Toffolon et al., 2010; Bozeman et al., 2024; Hayes et al., 2024). Notably, sub-daily variability is spatially heterogeneous and metric-dependent rather than monotonically damped downstream: for example, Kratie exhibits comparatively low sub-daily RBI but can still experience frequent rapid hourly rises during specific wet-season months (e.g., September 2019), underscoring the episodic nature of hydropeaking-relevant ramping.

4.2 Reverse flow threshold shifts and mechanistic interpretation

The most consequential system-level signal is the contraction and retiming of Tonle Sap reverse flow, expressed here as higher lag-adjusted discharge thresholds for onset and cessation and a shorter reverse flow season. Because reverse flow governs lake expansion and floodplain inundation (Ng and Park, 2021; Morovati et al., 2023), these shifts imply reduced duration of strong Mekong-lake connectivity, with likely consequences for sediment and nutrient exchange and for the seasonal availability of floodplain habitat.

Two mechanisms are likely acting together. First, changes in the shape and timing of the Mekong hydrograph–particularly weaker early wet-season rises and a more abrupt approach to peak flow–reduce the persistence of the hydraulic gradient required to initiate and sustain reversal. Second, local hydraulic and geomorphic changes in the confluence reach can modify conveyance and the head difference required for reversal (Quan et al., 2025). In particular, recent satellite-based estimates indicate that sand extraction from the Cambodian Mekong increased from ~24 Mt in 2016 to ~59 Mt in 2020, while natural sand supply in 2020 was only ~3.7 Mt, implying a large and persistent sediment deficit (Hackney et al., 2021). This deficit is associated with reach-scale bed incision (median ~−0.26 m yr^{-1} over 2013-2019) (Hackney et al., 2021) and intense local lowering near the confluence (net incision ~1.2 m yr^{-1}) (Hackney et al., 2025), providing a physically consistent pathway for threshold shifts via changes in cross-sectional geometry and stage-discharge relations.

A practical implication of the response-time framework is that it translates coupled dynamics into an operationally interpretable quantity: a lag-consistent Kratie discharge threshold associated with reverse flow initiation and termination. Because Kratie-to-confluence response time is short during high flow conditions, these thresholds are directly relevant for short-lead monitoring and for interpreting how changes in timing and variability–not only volume–affect Tonle Sap exchange.

4.3 Implications for ecosystems and governance

Although this study focuses on hydrology and does not model ecological outcomes directly, the documented shifts align with established pathways by which floodplain productivity can decline (Lambert and Koponen, 2008; Arias et al., 2012): shorter and less predictable connectivity, reduced floodplain access, and compressed inundation windows that can affect habitat heterogeneity and seasonal cues for fish movement and reproduction (Ngor et al., 2018; Sor et al., 2024; Chea et al., 2020;

Deng et al., 2023; Chevalier et al., 2023). These risks reinforce that "volume-only" perspectives are insufficient for basin planning. Effective transboundary management should explicitly consider (i) seasonal timing (onset/cessation), (ii) persistence and flashiness, and (iii) sub-daily ramping behavior, because each affects different components of floodplain-lake functioning and downstream risk.

4.4 Limitations and ways forward

While this study provides a holistic analysis of hydrological alterations across both long-term and sub-daily scales, several limitations remain that warrant further investigation. First, the attribution of observed sub-daily fluctuations to upstream hydropower operations is inherently constrained by the absence of publicly available dam release data (Morovati et al., 2026). Although the temporal alignment between wet-season peaks and sub-daily variability supports a linkage to hydropeaking, direct validation through operational records remains essential.

The interaction between river morphology, sediment loads, and hydraulic thresholds for reverse flow remains underrepresented. While the observed elevation in Kratie discharge thresholds aligns with regional bed incision and sand mining, spatially explicit bathymetric and sediment transport data are needed to robustly quantify their role.

While the comparison between measured (with-dam) and simulated no-dam scenarios reveals important shifts in flow memory, flashiness, and synchrony, it is important to acknowledge that uncertainty exists in the hydrological model used to simulate the no-dam scenario. Model uncertainties may influence flow amplitude and timing. Future work should quantify these uncertainties through ensemble simulations or data assimilation techniques.

This study focuses primarily on hydrological metrics and does not explicitly assess ecological or livelihood outcomes. Integrating these flow regime alterations with floodplain vegetation dynamics, fish migration cues, and agricultural timing would provide a more comprehensive view of cascading socio-ecological impacts.

5 Conclusion

This study provides a comprehensive spatiotemporal assessment of hydrological alterations in the Mekong River system and identifies extensive dam construction on both the mainstream and tributaries, together with climate change, as dominant drivers of the observed regime shifts. In the Tonle Sap system, sand mining emerges as an additional, locally important anthropogenic stressor that interacts with upstream flow regime change.

Hydrological metrics, including the Hurst exponent, flashiness index, and coefficient of variation, reveal that the Mekong mainstream is no longer functioning as a hydrologically coherent system. Regulation, dam sequencing, and associated interventions have fragmented longitudinal connectivity, particularly during the post-2010 mega-dam era. Consistent with this fragmentation, the synchrony of seasonal flow patterns has weakened along the river's longitudinal profile, with disrupted and locally distinct dynamics progressively replacing the previously unified flood pulse.

At Chiang Saen, annual minimum flows increased by 33.3% (from 748 $m^3 s^{-1}$ to 997 $m^3 s^{-1}$) in the post-dam period. A similar trend is observed downstream, most notably at Kratie, where minimum flows rose by 117.2% (from 1,326 $m^3 s^{-1}$ to 2,880 $m^3 s^{-1}$). In contrast, annual maximum flows decreased by 40% at Chiang Saen and by only 9.4% at Kratie, likely due to the buffering effects of monsoonal tributary inflows and dam operations on these tributaries.

These mainstream alterations propagate into the Tonle Sap system, where the reverse flow period is shortened by approximately 24 days in the post-dam period compared to the pre-dam baseline as a compound outcome of altered flow regime and local geomorphic change. The hydraulic trigger for reversal at the Mekong-Tonle Sap confluence is the local stage/head condition required to reverse the along-channel gradient, which is governed primarily by channel geometry and confluence hydraulics. Within this framework, sand mining-driven riverbed incision reduces confluence stage for a given discharge, thereby increasing the lag-adjusted Kratie discharge required to attain the confluence stage associated with reversal. Consistent with this mechanism, the median lag-adjusted Kratie discharge at reverse flow initiation increased from ~3,000 $m^3 s^{-1}$ (pre-dam) to ~7,000 $m^3 s^{-1}$ (post-dam), an increase of >130%. Superimposed on this shifted hydraulic setting, dam regulation and climate change reshape the seasonal hydrograph–dampening early wet season rises and altering flow timing and persistence–thereby reducing how frequently and how long the reversal-favourable confluence stage/head condition is exceeded. Together, these interacting drivers shorten and retime the reverse flow season.

The combined evidence of dampened high flows, pronounced episodic sub-daily variability in the recent record, and shifting seasonal flow timings points to a river system undergoing profound anthropogenic transformation. As regional development intensifies, future management must extend beyond annual water volume considerations, focusing instead on the temporal structure and synchrony of flow regimes–key to sustaining downstream ecosystems, floodplain agriculture, and rural livelihoods. Preserving the integrity of the Mekong-Tonle Sap flood pulse will require basin-wide hydrological monitoring, transparent data sharing, and coordinated transboundary water governance.

Code and data availability. Hydrological data, including water level and discharge data, are accessible at https://portal.mrcmekong.org/home (last access: 16 July 2025). Code for extracting canals across the lower Mekong can be obtained upon reasonable request from the primary author of the paper. FABDEM data is publicly available at https://www.fathom.global/product/global-terrain-data-fabdem/ (last access: 16 July 2025). Constructed DEM data for the Tonle Sap Lake and river can be obtained upon reasonable request from the primary author of the paper. Data of the reverse flow period is publicly available at https://pmfm.mrcmekong.org/monitoring/6b/ (last access: 17 July 2025).

Author contributions: KM conceptualized and designed the study. KM and FT contributed to model development, with KM responsible for model implementation and analysis. KM led the manuscript writing in close collaboration with HZ and FT. All authors contributed to discussions throughout the study, provided critical feedback, and approved the final version of the manuscript.

Competing interests. At least one of the (co-)authors is a member of the editorial board of Hydrology and Earth System Sciences.

Acknowledgment. This research was supported by the Shuimu Tsinghua Scholar Program. The authors confirm that no portion of this manuscript was generated or assisted by AI tools. The authors thank two anonymous reviewers for their constructive comments and suggestions.

References

Ang, W. J., Park, E., Pokhrel, Y., Tran, D. D., and Loc, H. H.: Dams in the Mekong: a comprehensive database, spatiotemporal distribution, and hydropower potentials, Earth Syst. Sci. Data, 16, 1209–1228, https://doi.org/10.5194/essd-16-1209-2024, 2024.

Arias, M. E., Cochrane, T. A., Kummu, M., Lauri, H., Holtgrieve, G. W., Koponen, J., Piman, T: Impacts of hydropower and climate change on drivers of ecological productivity of Southeast Asia's most important wetland. *Ecological modelling*, *272*, 252-263, https://doi.org/10.1016/j.ecolmodel.2013.10.015, 2014.

Arias, M. E., Cochrane, T. A., Norton, D., Killeen, T. J., Khon, P: The flood pulse as the underlying driver of vegetation in the largest wetland and fishery of the Mekong Basin. Ambio, 42, 864-876, https://doi.org/10.1007/s13280-013-0424-4, 2013.

Arias, M. E., Cochrane, T. A., Piman, T., Kummu, M., Caruso, B. S., & Killeen, T. J: Quantifying changes in flooding and habitats in the Tonle Sap Lake (Cambodia) caused by water infrastructure development and climate change in the Mekong Basin. Journal of Environmental Management, 112, 53-66, https://doi.org/10.1016/j.jenvman.2012.07.003, 2012.

Arthington, A. H., Bhaduri, A., Bunn, S. E., Jackson, S. E., Tharme, R. E., Tickner, D., Ward, S: The Brisbane declaration and global action agenda on environmental flows. *Frontiers in Environmental Science*, *6*, 45, https://doi.org/10.3389/fenvs.2018.00045, 2018.

Baran, E., Myschowoda, C: Dams and fisheries in the Mekong Basin. Aquatic Ecosystem Health & Management, 12(3), 227-234, https://doi.org/10.1080/14634980903149902, 2009.

Binh, V. D., Kantoush, S. A., Saber, M., Mai, N. P., Maskey, S., Phong, D. T., Sumi, T: Long-term alterations of flow regimes of the Mekong River and adaptation strategies for the Vietnamese Mekong Delta. Journal of Hydrology: Regional Studies, 32, 100742, https://doi.org/10.1016/j.ejrh.2020.100742, 2020.

Blöschl, G., Sivapalan, M: Process controls on regional flood frequency: Coefficient of variation and basin scale. *Water Resources Research*, *33*(12), 2967-2980, https://doi.org/10.1029/97WR00568, 1997.

Bozeman, B. B., Pracheil, B. M., & Matson, P. G. (2025). The environmental impact of hydropower: a systematic review of the ecological effects of sub-daily flow variability on riverine fish. Reviews in Fish Biology and Fisheries, 35(1), 45-76, https://doi.org/10.1007/s11160-024-09909-4

Bunn, S. E., Arthington, A. H. (2002). Basic principles and ecological consequences of altered flow regimes for aquatic biodiversity. Environmental management, 30(4), 492-507, https://doi.org/10.1007/s00267-002-2737-0

Chea, R., Pool, T. K., Chevalier, M., Ngor, P., So, N., Winemiller, K. O., ... & Grenouillet, G. (2020). Impact of seasonal hydrological variation on tropical fish assemblages: abrupt shift following an extreme flood event. Ecosphere, 11(12), e03303, https://doi.org/10.1002/ecs2.3303

Chen, A., Liu, J., Kummu, M., Varis, O., Tang, Q., Mao, G., Chen, D: Multidecadal variability of the Tonle Sap Lake flood pulse regime. *Hydrological Processes*, *35*(9), e14327, https://doi.org/10.1002/hyp.14327, 2021.

Chevalier, M., Ngor, P. B., Pin, K., Touch, B., Lek, S., Grenouillet, G., & Hogan, Z. (2023). Long-term data show alarming decline of majority of fish species in a Lower Mekong basin fishery. Science of the Total Environment, 891, 164624, https://doi.org/10.1016/j.scitotenv.2023.164624

Chua, S. D. X., Lu, X. X., Oeurng, C., Sok, T., and Grundy-Warr, C.: Drastic decline of flood pulse in the Cambodian floodplains (Mekong River and Tonle Sap system), Hydrol. Earth Syst. Sci., 26, 609–625, https://doi.org/10.5194/hess-26-609-2022, 2022.

Cochrane, T. A., Arias, M. E., & Piman, T: Historical impact of water infrastructure on water levels of the Mekong River and the Tonle Sap system. Hydrology and Earth System Sciences, 18(11), 4529-4541, https://doi.org/10.5194/hess-18-4529-2014, 2014.

Dang, H., Pokhrel, Y., Shin, S., Stelly, J., Ahlquist, D., Du Bui, D: Hydrologic balance and inundation dynamics of Southeast Asia's largest inland lake altered by hydropower dams in the Mekong River basin. *Science of the Total Environment*, *831*, 154833, https://doi.org/10.1016/j.scitotenv.2022.154833, 2022.

Deng, Q., Sabo, J. L., Holtgrieve, G. W., Ngor, P. B., & Holway, J. (2023). Timing of hydrologic anomalies direct impacts on migration traits in a flood pulse fishery system. Journal of Applied Ecology, 60(3), 494-506, https://doi.org/10.1111/1365-2664.14349

Delgado, J. M., Apel, H., & Merz, B: Flood trends and variability in the Mekong river. *Hydrology and Earth System Sciences*, *14*(3), 407-418, https://doi.org/10.5194/hess-14-407-2010, 2010.

Deltares: Delft3D-Flow user manual (https://content.oss.deltares.nl/delft3d4/Delft3D-FLOW_User_Manual.pdf (last access: 10 July 2025). 2025.

Do, S. K., Du, T. L., Lee, H., Chang, C. H., Bui, D. D., Nguyen, N. T., Bui, L. K: Assessing impacts of hydropower development on downstream inundation using a hybrid modeling framework integrating satellite data-driven and process-based models. *Water Resources Research*, *61*(3), e2024WR037528, https://doi.org/10.1029/2024WR037528, 2025.

Dudgeon, D: Multiple threats imperil freshwater biodiversity in the Anthropocene. Current Biology, 29(19), R960-R967, DOI: 10.1016/j.cub.2019.08.002, 2019.

Duc, N. A., Nguyen, L. T., Thai, T. H., Khan, A., Rautenstrauch, K., Schmidt, C: Assessing cumulative impacts of the proposed Lower Mekong Basin hydropower cascade on the Mekong River floodplains and Delta–Overview of integrated modeling methods and results. *Journal of Hydrology*, *581*, 122511, https://doi.org/10.1016/j.jhydrol.2018.01.029, 2020.

Gannon, J. P., Kelleher, C., Zimmer, M: Controls on watershed flashiness across the continental US. *Journal of Hydrology*, *609*, 127713, https://doi.org/10.1016/j.jhydrol.2022.127713, 2022.

Hackney, C. R., Cisneros, J., Heng, S., Darby, S. E., Leyland, J., Konsoer, K., Parsons, D. R: Increased hydraulic roughness in alluvial rivers created by sand-mining sculpted bed features. *Journal of Geophysical Research: Earth Surface*, *130*(6), e2024JF008189, https://doi.org/10.1029/2024JF008189, 2025.

Hackney, C. R., Vasilopoulos, G., Heng, S., Darbari, V., Walker, S., and Parsons, D. R.: Sand mining far outpaces natural supply in a large alluvial river, Earth Surf. Dynam., 9, 1323–1334, https://doi.org/10.5194/esurf-9-1323-2021, 2021.

Hecht, J. S., Lacombe, G., Arias, M. E., Dang, T. D., Piman, T: Hydropower dams of the Mekong River basin: A review of their hydrological impacts. *Journal of hydrology*, *568*, 285-300, https://doi.org/10.1016/j.jhydrol.2018.10.045, 2019.

Hayes, D. S., Bätz, N., Tonolla, D., Merl, K., Auer, S., Gorla, L., ... & Greimel, F. (2025). Why hydropeaking frequency matters: effects of recurring stranding on fish. Journal of Ecohydraulics, 10(3), 302-318, https://doi.org/10.1080/24705357.2024.2426820

Khan, A., Hussain, S., Bakhet, A., Anwer, A., Raza, S. M., Ali, S., Zakarya, M: Climate time series variability analysis of Islamabad Capital Territory using fractal dimension and Hurst exponent methods. *Journal of Atmospheric and Solar-Terrestrial Physics*, *267*, 106406, https://doi.org/10.1016/j.jastp.2024.106406, 2025.

Kummu, M., Tes, S., Yin, S., Adamson, P., Józsa, J., Koponen, J., Sarkkula, J: Water balance analysis for the Tonle Sap Lake–floodplain system. *Hydrological Processes*, *28*(4), 1722-1733, https://doi.org/10.1002/hyp.9718, 2014.

Lamberts, D., & Koponen, J. (2008). Flood pulse alterations and productivity of the Tonle Sap ecosystem: a model for impact assessment. AMBIO: A Journal of the Human Environment, 37(3), 178-184, https://doi.org/10.1579/0044-7447(2008)37[178:FPAAPO]2.0.CO;2

Lao, J., Wang, C., Nie, S., Xi, X., & Wang, J: Monitoring and analysis of water level changes in Mekong River from ICESat-2 spaceborne laser altimetry. *Water*, *14*(10), 1613, https://doi.org/10.3390/w14101613, 2022.

Lauri, H., de Moel, H., Ward, P. J., Räsänen, T. A., Keskinen, M., Kummu, M: Future changes in Mekong River hydrology: impact of climate change and reservoir operation on discharge. *Hydrology and Earth system sciences*, *16*(12), 4603-4619, https://doi.org/10.5194/hess-16-4603-2012, 2012.

LMC-MRCs Technical report – Phase 1 of the Joint study on the changing patterns of hydrological conditions of the Lancang-Mekong River Basin and adaptation strategies. Beijing: LMC Water Center and Vientiane: MRC Secretariat. DOI: 10.52107/mrc.bc3v7s (https://www.mrcmekong.org/publications/technical-report-phase-1-of-the-joint-study-on-the-changing-patterns-of-hydrological-conditions-of-the-lancang-mekong-river-basin-and-adaptation-strategies/) (last access: 10 July 2025), 2023.

Li, D., Long, D., Zhao, J., Lu, H., Hong, Y: Observed changes in flow regimes in the Mekong River basin. Journal of Hydrology, 551, 217-232, https://doi.org/10.1016/j.jhydrol.2017.05.061, 2017.

Li, W., Maharjan, S., El-Askary, H: Atmospheric teleconnection patterns and hydrological whiplashes in the Western US. Scientific Reports, 15(1), 21262, https://doi.org/10.1038/s41598-025-06087-6, 2025.

Lu, X. X., Chua, S. D. X: River discharge and water level changes in the Mekong River: Droughts in an era of mega-dams. Hydrological Processes, 35(7), e14265, https://doi.org/10.1002/hyp.14265, 2021.

Lyu, H., Morovati, K., Zhang, K., Tian, F: Hydrological model calibration in data-deficient basins using satellite altimetry and a hydrodynamic model. *Journal of Hydrology*, *643*, 132022, https://doi.org/10.1016/j.jhydrol.2024.132022, 2024.

Lu, X. X., Li, S., Kummu, M., Padawangi, R., Wang, J. J: Observed changes in the water flow at Chiang Saen in the lower Mekong: Impacts of Chinese dams?. *Quaternary International*, *336*, 145-157, https://doi.org/10.1016/j.quaint.2014.02.006, 2014.

Morovati, K., Tian, F., Pokhrel, Y., Someth, P., Shi, L., Zhang, K., Ly, S: Fishery and agriculture amidst human activities and climate change in the Mekong River: A review of gaps in data and effective approaches towards sustainable development. *Journal of Hydrology*, 132043, https://doi.org/10.1016/j.jhydrol.2024.132043, 2024a.

Morovati, K., Tian, F., Kummu, M., Shi, L., Tudaji, M., Nakhaei, P., Olivares, M. A: Contributions from climate variation and human activities to flow regime change of Tonle Sap Lake from 2001 to 2020. *Journal of Hydrology*, *616*, 128800, https://doi.org/10.1016/j.jhydrol.2022.128800, 2023.

Morovati, K., Nakhaei, P., Tian, F., Tudaji, M., Hou, S: A Machine learning framework to predict reverse flow and water level: A case study of Tonle Sap Lake. *Journal of Hydrology*, *603*, 127168, https://doi.org/10.1016/j.jhydrol.2021.127168, 2021.

Morovati, K., Zhang, K., Shi, L., Pokhrel, Y., Wu, M., Someth, P., Ly, S., Tian, F.: On the cause of large daily river flow fluctuations in the Mekong River, Hydrol. Earth Syst. Sci., 28, 5133–5147, https://doi.org/10.5194/hess-28-5133-2024, 2024b.

Morovati, K., Kondolf, G. M., Pokhrel, Y., Tian, F: Saving Mekong River's ecosystem integrity before delta sinks. Science bulletin, S2095-9273. https://doi.org/10.1016/j.scib.2026.01.031

MRC: The Council Study: Impacts of water infrastructure development on the Mekong mainstream. MRC Secretariat, Vientiane (last access: 10 July 2025: https://www.mrcmekong.org/wp-content/uploads/2024/08/macroeconomic-assessment-report-of-the-MRC-Council-Study.pdf), 2017.

MRC: Hydropower Mitigation Guidelines (Volume 3), Vientiane: MRC Secretariat, https://www.mrcmekong.org/wpcontent/uploads/2024/08/Ish0306-vol3-1.pdf (last access: 26 November 2024), 2020.

Nan, Y., Tian, L., He, Z., Tian, F., and Shao, L.: The value of water isotope data on improving process understanding in a glacierized catchment on the Tibetan Plateau, Hydrol. Earth Syst. Sci., 25, 3653–3673, https://doi.org/10.5194/hess-25-3653-2021, 2021.

Ng, W. X., & Park, E. (2021). Shrinking Tonlé Sap and the recent intensification of sand mining in the Cambodian Mekong River. Science of the Total Environment, 777, 146180, https://doi.org/10.1016/j.scitotenv.2021.146180

Ngor, P. B., Oberdorff, T., Phen, C., Baehr, C., Grenouillet, G., & Lek, S. (2018). Fish assemblage responses to flow seasonality and predictability in a tropical flood pulse system. Ecosphere, 9(11), e02366, https://doi.org/10.1002/ecs2.2366

Nguyen, T. T. H., Wang, Y. L., Binh, D. V., Dang, T. D: Hydrological alterations and sediment changes caused by dams in the Mekong River Basin. *Hydrological Sciences Journal*, 1-17, https://doi.org/10.1080/02626667.2025.2498684, 2025.

Orieschnig, C., Adla, S., Pan Chun, K., Srivastava, S., et al.: Effective science communication in the face of water crises: a community perspective on challenges and best practice in HELPING, Hydrol. Sci. J., 2026, https://doi.org/10.1080/02626667.2026.2625282.

Piman, T., Lennaerts, T., Southalack, P: Assessment of hydrological changes in the lower Mekong Basin from Basin-Wide development scenarios. *Hydrological Processes*, *27*(15), 2115-2125, https://doi.org/10.1002/hyp.9764, 2013.

Poff, N.L., Allan, J.D., Bain, M.B., Karr, J.R., Prestegaard, K.L., Richter, B.D., Stromberg, J. C: The natural flow regime. Bioscience 47 (11), 769–784, https://doi.org/10.2307/1313099, 1997.

Poff, N. L., Olden, J. D., Merritt, D. M., Pepin, D. M: Homogenization of regional river dynamics by dams and global biodiversity implications. *Proceedings of the National Academy of Sciences*, *104*(14), 5732-5737, https://doi.org/10.1073/pnas.0609812104, 2007.

Pokhrel, Y., Burbano, M., Roush, J., Kang, H., Sridhar, V., Hyndman, D. W: A review of the integrated effects of changing climate, land use, and dams on Mekong river hydrology. *Water*, *10*(3), 266, https://doi.org/10.3390/w10030266, 2018.

Quan, L. Q., Hackney, C. R., Vasilopoulos, G., Coulthard, T., Hung, N. N., Darby, S. E., & Parsons, D. R. (2025). Sand-mining-driven reduction in Tonle Sap Lake's critical flood pulse. Nature Sustainability, 1-12, https://doi.org/10.1038/s41893-025-01677-8

Räsänen, T. A., Someth, P., Lauri, H., Koponen, J., Sarkkula, J., Kummu, M: Observed river discharge changes due to hydropower operations in the Upper Mekong Basin. *Journal of hydrology*, *545*, 28-41, https://doi.org/10.1016/j.jhydrol.2016.12.023, 2017.

Sabo, J. L., Ruhi, A., Holtgrieve, G. W., Elliott, V., Arias, M. E., Ngor, P. B., ... & Nam, S. (2017). Designing river flows to improve food security futures in the Lower Mekong Basin. Science, 358(6368), eaao1053, DOI: 10.1126/science.aao105.

Shi, L., Sun, J., Lin, B., Morovati, K., Liu, Z., Zuo, X: Macroscopic hydro-thermal processes in a large channel-type reservoir. *Journal of Hydrology: Regional Studies*, *47*, 101367, https://doi.org/10.1016/j.ejrh.2023.101367, 2023.

Sor, R., Prudencio, L., Hogan, Z. S., Chandra, S., Ngor, P. B., & Null, S. E. (2024). Factors influencing fish migration in one of the world's largest inland fisheries. Frontiers in Freshwater Science, 2, 1426350, https://doi.org/10.3389/ffwsc.2024.1426350

Soukhaphon, A., Baird, I. G., & Hogan, Z. S: The impacts of hydropower dams in the Mekong River Basin: A review. *Water*, *13*(3), 265, https://doi.org/10.3390/w13030265, 2021.

Toffolon, M., Siviglia, A., & Zolezzi, G. (2010). Thermal wave dynamics in rivers affected by hydropeaking. Water Resources Research, 46(8), https://doi.org/10.1029/2009WR008234

Try, S., Sayama, T., Oeurng, C., Sok, T., Ly, S., Uk, S: Identification of the spatio-temporal and fluvial-pluvial sources of flood inundation in the Lower Mekong Basin. *Geoscience Letters*, *9*(1), 5, https://doi.org/10.1186/s40562-022-00215-0, 2022.

Try, S., Tanaka, S., Tanaka, K., Sayama, T., Lee, G., Oeurng, C: Assessing the effects of climate change on flood inundation in the lower Mekong Basin using high-resolution AGCM outputs. Progress in Earth and Planetary Science, 7(1), 34, https://doi.org/10.1186/s40645-020-00353-z, 2020.

United Nations: UN Comtrade Database, available at: https://comtrade.un.org (last access: 10 July 2025), 2017.

Yin, X. A., Yang, Z. F., Petts, G. E: Reservoir operating rules to sustain environmental flows in regulated rivers. *Water Resources Research*, *47*(8), https://doi.org/10.1029/2010WR009991, 2011.

Yoshida, Y., Lee, H. S., Trung, B. H., Tran, H. D., Lall, M. K., Kakar, K., Xuan, T. D: Impacts of mainstream hydropower dams on fisheries and agriculture in lower Mekong Basin. *Sustainability*, *12*(6), 2408, https://doi.org/10.3390/su12062408, 2020.

Yun, X., Song, J., Wang, J., Bao, H: Modelling to assess the suitability of hydrological-hydrodynamic model under the hydropower development impact in the Lancang-Mekong River basin. *Journal of Hydrology*, *637*, 131393, https://doi.org/10.1016/j.jhydrol.2024.131393, 2024.

Wang, J., Yun, X., Pokhrel, Y., Yamazaki, D., Zhao, Q., Chen, A., Tang, Q: Modeling daily floods in the Lancang-Mekong River basin using an improved hydrological-hydrodynamic model. *Water Resources Research*, *57*(8), e2021WR029734, https://doi.org/10.1029/2021WR029734, 2021.

Wu, M., Sun, J., Shi, L., Guo, J., Morovati, K., Lin, B., Li, Y: Vertical water renewal and dissolved oxygen depletion in a semi-enclosed Sea. *Journal of Hydrology*, *637*, 131369, https://doi.org/10.1016/j.jhydrol.2024.131369, 2024.

Zhang, K., Morovati, K., Tian, F., Yu, L., Liu, B., Olivares, M. A: Regional contributions of climate change and human activities to altered flow of the Lancang-mekong river. *Journal of Hydrology: Regional Studies*, *50*, 101535, https://doi.org/10.1016/j.ejrh.2023.101535, 2023.

Zhao, H., Tian, F., Zhang, K., Morovati, K., Sun, J: Intelligent remote sensing canal system detection and irrigation water use estimation: A case study in the transboundary Mekong River Basin. *Journal of Hydrology*, *657*, 133110, https://doi.org/10.1016/j.jhydrol.2025.133110, 2025.